Chinese Chemical Letters 34 (2023) 107794

Contents lists available at ScienceDirect

Chinese Chemical Letters

journal homepage: www.elsevier.com/locate/cclet

Ultrabroad-band, white light emission from carbon dot-based materials with hybrid fluorescence/phosphorescence for single component white light-emitting diodes

Yuchen Li[a,1], Qijun Li[b,1,*], Shuai Meng[a], Yukun Qin[c], Dengke Cheng[a], Hailing Gu[a], Zifei Wang[d], Yunxia Ye[a], Jing Tan[a,*]

[a] Institute of Micro-nano Optoelectronics and Terahertz Technology, School of Mechanical Engineering, Jiangsu University, Zhenjiang 212013, China
[b] School of Mechanical Engineering, Yangzhou University, Yangzhou 225009, China
[c] Institute for Energy Research, Jiangsu University, Zhenjiang 212013, China
[d] School of Materials Science & Engineering, Qilu University of Technology (Shandong Academy of Sciences), Ji'nan 250300, China

ARTICLE INFO

Article history:
Received 7 June 2022
Revised 1 September 2022
Accepted 1 September 2022
Available online 5 September 2022

Keywords:
Carbon dots
White LEDs
Fluorescence/phosphorescence dual emission
Ultrabroad-band
Conjugation structure

ABSTRACT

Benefiting from the large Stokes shift between fluorescence and phosphorescence, fluorescence/phosphorescence dual-emitting carbon dots (CDs) have gradually entered at the stage of single-phase white light-emitting diodes (WLEDs) as 'green material'. However, most of the developed dual-emitting CDs have weak phosphorescence, short emission wavelength and narrow emission band, resulting in relatively bluish white light emission and low color rendering index (CRI). Herein, an ultrabroad-band fluorescence/phosphorescence dual-emitting CD-based material (UB-CD@BA) is prepared by thermal treatment of boric acid (BA) and CDs with large conjugated structure. The stable covalent bonding between CDs and BA, as well as three-dimensional spatial restriction effect of self-polymerization BA molecules around CDs during long-term heating efficiently rigidified the single/triplet excited states of CDs from non-radiative deactivation, thus producing strong dual emissive materials with the high phosphorescence quantum yield of 21%. Remarkable, the prepared UB-CD@BA powders exhibit bright pure white light emission with Commission Internationale de l'Eclairage (CIE) coordinates of (0.32, 0.33) and the highest reported full width at half maximum of 250 nm. Based on the unique characteristics of UB-CD@BA, it was used as a color conversion layer to prepare a WLED with CIE coordinates of (0.35, 0.33) and the CRI value of 87.

With the advent of the low-carbon economy, white light-emitting diodes (WLEDs) have received great attention for their advantages such as low power consumption, remarkable energy efficiency, simple driving, and long operational life [1–5]. In the design of WLEDs, phosphors, as color conversion layers, play a key role in determining the performance parameters, such as color rendering index (CRI), correlated color temperature (CCT) and Commission Internationale de l'Eclairage (CIE) chromaticity coordinates. So far, most WLEDs developed have been fabricated by combining multi-component materials with emission color covering the entire visible range [6–8]. Compared with these combined emitters, a single-component white light emitting phosphor is very promising for WLEDs due to their superior performance of less phase segregation, no color aging and improved stability [9–11]. However, efficient single-component white light emission materials mainly demonstrated in some rare-earth-based phosphors and semiconductor quantum dots, they usually suffer from drawbacks of heavy-metal cytotoxicity, scarcity of their precursors, and/or complicated preparation procedures [12,13].

Carbon dots (CDs) as a recently emerged class of luminescent nanomaterials have attracted enormous attention due to their excellent optical performance, cost-effective preparation and low toxicity [14–24]. Recently, fluorescence/phosphorescence dual emissive single-component white emissive CDs materials have been demonstrated as promising phosphors for WLEDs, due to the large Stokes shift between fluorescence and phosphorescence [25–31]. In 2019, Yang *et al.* reported the first demonstration of fluorescence/phosphorescence dual emission single-component white CDs with 25% total quantum efficiency (QY) and a yellow phosphorescence quantum efficiency (PQY) of 6% [32]. Wang *et al.* prepared

* Corresponding authors.
E-mail addresses: liqijun0606@163.com (Q. Li), tanjing@ujs.edu.cn (J. Tan).
[1] These authors contributed equally to this work.

https://doi.org/10.1016/j.cclet.2022.107794
1001-8417/

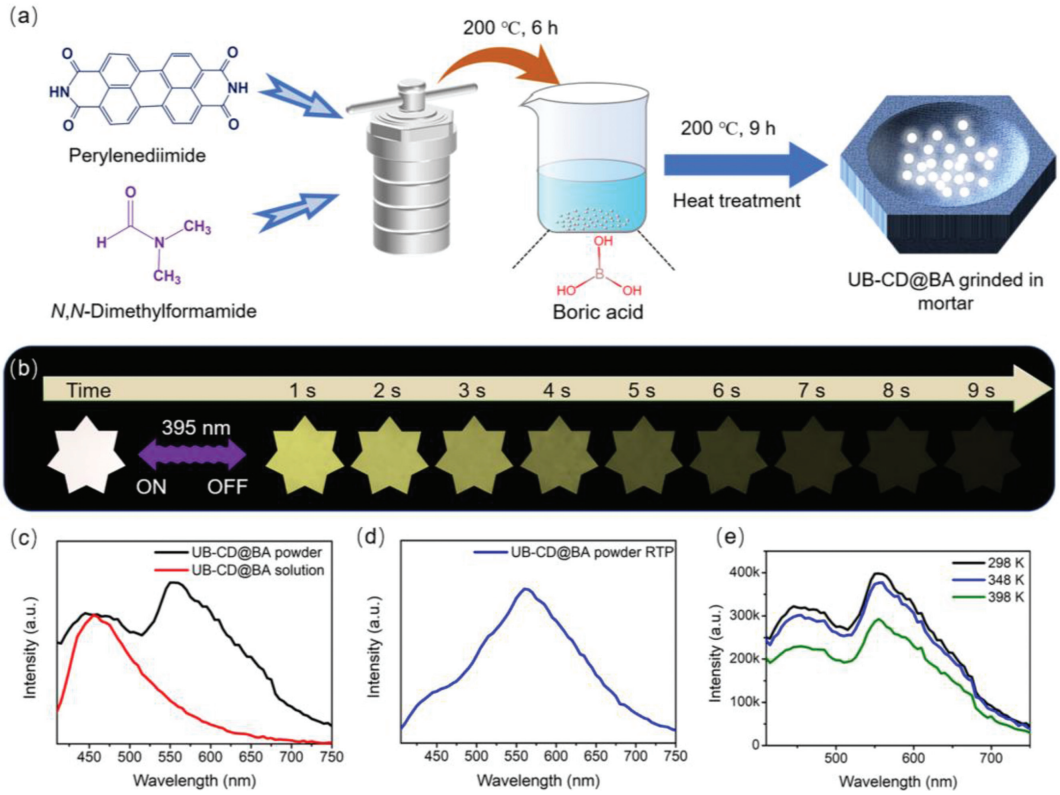

Fig. 1. (a) Illustration of UB-CD@BA synthesis route. (b) Images of UB-CD@BA before and after being irradiated by 395 nm UV lamp under ambient conditions. (c) Fluorescence spectra of UB-CD@BA powders and aqueous solution upon excitation at 395 nm, respectively. (d) Phosphorescence spectrum of UB-CD@BA powders under 395 nm excitation. (e) Fluorescence spectra of UB-CD@BA powders at different temperature under 395 nm excitation.

white emissive CDs and developed an ultraviolet (UV)-pumped CD-based WLED with CIE coordinates (0.268, 0.346) and a CRI of 85.3 by combining the CDs with blue fluorescence and green phosphorescence emissive CDs [33]. However, their phosphorescence emissive intensities were extremely lower compared to their fluorescence, leading to a narrow emission band and cold white light.

Most recently, our group reported a single white light emissive CDs material with a comparable fluorescence and phosphorescence emission intensity *via* incorporating CDs into boric acid (BA) matrix [34]. However, their phosphorescent emission peak was in the green region. The short emission wavelength (<520 nm) and narrow emission band (full width at half maximum < 180 nm) of phosphorescence caused the relatively bluish white light emission and the low CRI. Therefore, it is imperative to promote phosphorescence emission intensity and achieve the phosphorescence emission band at long wavelengths region to further broaden the emission band.

Selecting compounds with large conjugated structures as precursors for CDs synthesis is an effective method to obtain long-wavelength phosphorescence. Perylene imide derivatives with large conjugated structure have been widely used in perovskite solar energy and photocatalysis, but it has not been used as a precursor to synthesize phosphorescent CDs [35–38]. In this work, an ultrabroad-band white light emissive CD-based material (UB-CD@BA) with efficient RTP centered at 560 nm, and the full width at half-maximum (FWHM) over 250 nm covering the entire visible spectral window from 400 nm to 750 nm was synthesized by a long-term thermal melting BA and CDs prepared from perylene imide derivatives. During annealed process, the strong confinement and stable covalent bonding are formed between CDs and BA matrix, which suppress the non-radiative transition, promote inter-system crossing and prevent aggregation-induced quenching in the solid state. Multiple structural confinements effect greatly promote the fluorescence and phosphorescence emission with overall QY of 28%, especially for PQY up to 21%, leading to the ultrabroad-band and pure white light emission. In addition, the obtained UB-CD@BA shows an ultrahigh QY of 52% under 505 nm light excitation. Combing with the excellent optical property, a WLED based on a single-color converter of CDs phosphors was fabricated with a CRI of 87 and CIE coordinates of (0.35, 0.33).

The CDs were synthesized by one-pot solvothermal treatment of 3,4,9,10-perylenetetracarboxylic diimide at 200 °C for 6 h, and then composited with BA through thermal melting at 200 °C for 9 h to prepare UB-CD@BA (Fig. 1a). In order to obtain an optimal photoluminescence performance, different ratios of CDs and BA for preparing UB-CD@BA were screened. As shown in Table S1 (Supporting information), the CIE coordinates of sample from the ratio of 0.066% (*i.e.*, CDs to BA by weight) are (0.32, 0.33), which is closest to the standard white light (0.33, 0.33), and the corresponding product is taken to discuss in this study.

The UB-CD@BA powders exhibit bright white light emission under a UV lamp (395 nm) and yellow phosphorescence after ceasing the UV irradiation (Fig. 1b and Fig. S1 in Supporting information). In fluorescence spectra, the UB-CD@BA powders show obvious dual emission peak centered at about 450 and 560 nm with record broad FWHM over 250 nm covering the entire visible spectral window from 400 nm to 750 nm under the excitation of 395 nm light (Fig. 1c). As far as we know, this is the highest value among CD-based white light emissive materials (Table S2 in Supporting information). Different from the previously reported dual emissive CDs, the UB-CD@BA powders exhibits obvious bimodal emission of blue fluorescence and yellow phosphorescence, where the phosphorescence intensity is comparable to that of flu-

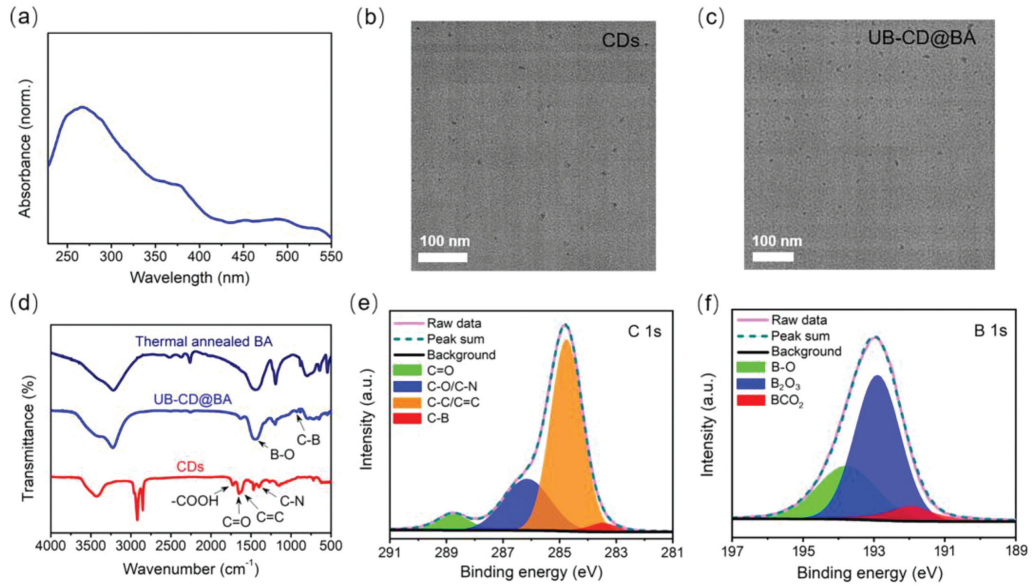

Fig. 2. (a) The UV-visible absorption spectrum of UB-CD@BA powders. (b, c) TEM images of CDs and UB-CD@BA, respectively. (d) FTIR spectra of CDs, UB-CD@BA and thermal annealed BA. High-resolution C 1s (e) and B 1s (f) XPS spectra of UB-CD@BA, respectively.

orescence, thus leading to pure white-light emission. When UB-CD@BA powders are fully dissolved in water, the peak at 560 nm nearly disappears accompanied by the disappearance of phosphorescence, while the emission centered at 450 nm still exists in fluorescence spectrum (Fig. 1c). Moreover, the emission centered at 560 nm in the phosphorescence spectrum of UB-CD@BA almost coincides with its peak in the fluorescence spectrum (Fig. 1d). Considering that phosphorescence can be quenched by dissolved oxygen in water and solvent-assisted relaxation, we conclude that the peak at 560 nm in the fluorescence spectrum is mainly derived from phosphorescence. The temperature-dependent fluorescence spectra (Fig. 1e) and phosphorescence spectra (Fig. S2 in Supporting information) of UB-CD@BA powders show that the emission intensity of the peak at 560 nm decreases with increasing temperature, further confirming their phosphorescence nature. In addition, phosphorescence behavior of thermal annealed BA powders was investigated (Fig. S3 in Supporting information). The thermal annealed BA matrix exhibited very weak phosphorescence compared to that of UB-CD@BA at room temperature, which indicates that the high-efficiency RTP mainly comes from the contribution of CDs rather than the BA. Under 395 nm light excitation, UB-CD@BA powders exhibited total QY of 28% and PQY 21%, respectively.

The UV–vis absorption spectrum (Fig. 2a) of UB-CD@BA powders exhibited broader absorption band and a distinct absorption tail extending to the visible region, indicating large conjugated structure in CDs, which maybe inherited from large conjugated perylene imide. The fluorescence excitation spectrum of UB-CD@BA powders exhibits a broad peak at 400–550 nm (Fig. S4 in Supporting information), which is accordance with the absorption band of the large conjugate structure in CDs. Under 505 nm light excitation, UB-CD@BA powders exhibit total QY of 52%. In addition, UB-CD@BA powders show an excitation-dependent phosphorescence (Fig. S5 in Supporting information). With the increase of the excitation wavelength, the phosphorescence emission is gradually red-shifted. Under the excitation of 455 nm, the UB-CD@BA powders can emit orange-red phosphorescence, which is very rare phenomenon. It should be pointed out that such phosphorescence with long wavelength excitation and emission is usually attributed to large conjugated structures.

In order to reveal the origin of high-efficiency and broad solid-state luminescence, the chemical structure and photophysical properties of CDs before and after embedding in BA were investigated. The transmission electron microscopy (TEM) image (Fig. 2b) demonstrates that the CDs show a uniform quasi-spherical shape with a comparable average diameter of 5 ± 1.2 nm. The Fig. 2c shows that the morphology and size of CDs after embedding in BA were not significantly changed. The X-ray diffraction (XRD) pattern of CDs (Fig. S6 in Supporting information) has a broad peak at around $2\theta = 22°$, which is corresponded to the typical peak of CDs as previously reported [39]. In Fourier transform infrared (FTIR) spectra (Fig. 2d and Fig. S7 in Supporting information), perylene imide precursor exhibits absorption bands at 1684, 1594 and 1355 cm^{-1}, which correspond to the stretching vibrations of C=O, perylene ring and C–N, respectively [40,41]. These characteristic absorption peaks are slightly shifted in the FTIR spectra of CDs, which indicates the formation of an extended conjugation of the precursor into CDs during the carbonization process. Compared to the precursor, new absorption band at approximately 1723 cm^{-1} corresponding to the carboxylic acid groups appeared, which is mainly attributed to the increase of the oxidation degree of CDs. After heat treatment of CDs and BA matrix, new absorption peaks at about 927 and 1439 cm^{-1} are attributed to the stretching vibration of C–B and B–O bonds, respectively [42–46]. The structural analysis based on X-ray photoelectron spectroscopies (XPS) further confirmed the FTIR results. The high-resolution (HR) spectrum of C 1s of UB-CD@BA (Fig. 2e) have four bands centered at 288.8, 286.2, 284.8 and 283.5 eV, which belong to C=O, C–O/C–N, C–C/C=C and C–B, respectively. Comparing the XPS spectra of UB-CD@BA with the original CDs, thermal treatment resulted in the appearance of B 1s peak (Fig. 2f). The HR B 1s spectrum of UB-CD@BA can be fitted to three bands centered at 193.8, 192.9 and 192 eV, which belong to B–O, B_2O_3 and BCO_2, respectively, implying the dehydration process occurs between CDs and BA molecules [34,44,45,47]. These results clearly demonstrate the formation of CDs with large conjugated structure, and CDs were tightly immobilized in BA matrix by the confined effect.

In order to further clarify the confined effect of the BA, we prepared UB-CD@BA powders at 200 °C at different reaction times at the following intervals from 1.5, 6, 9 and 12 h, denoted as UB-

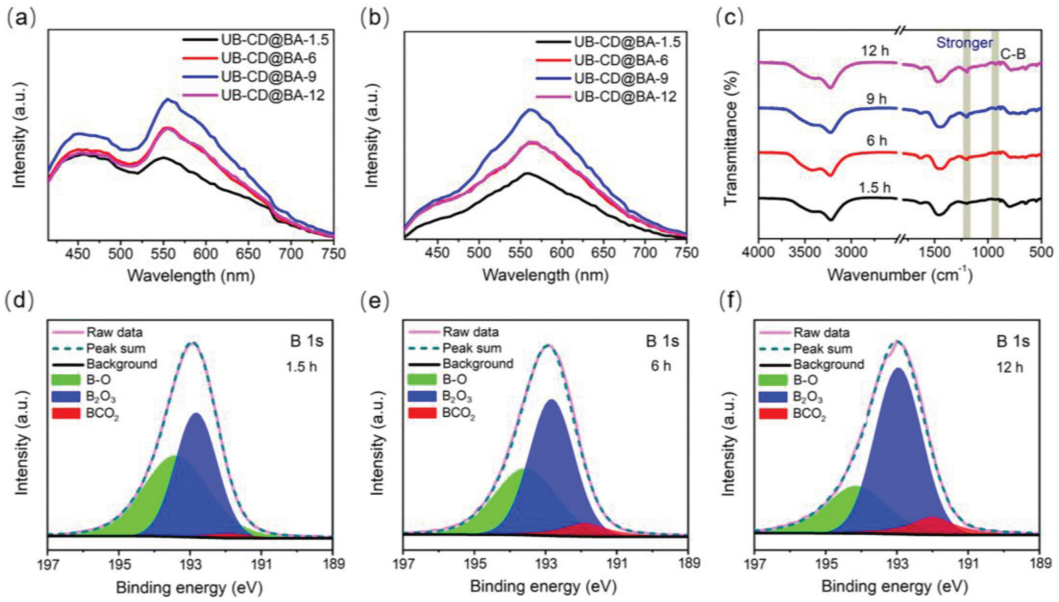

Fig. 3. (a, b) Fluorescence and phosphorescence spectra of UB-CD@BA at different reaction times, respectively. (c) FTIR spectra of UB-CD@BA-X. ~~(d, e)~~ XPS high-resolution B 1s spectra of UB-CD@BA-1.5 (d), UB-CD@BA-6 (e), UB-CD@BA-12 (f), respectively.

CD@BA-X (X = 1.5, 6, 9, 12). As shown in Figs. 3a and b, with reaction time increased from 1.5 h to 9 h, the fluorescence and phosphorescence intensity of as-synthesized composites became stronger and the phosphorescence average lifetime (Fig. S8 and Table S3 in Supporting information) also extended from 0.59 s to 1.11 s, suggesting that the interaction between CDs and BA might have changed with prolonged heating time. FTIR spectra of the synthesized samples show that the absorption of C−B at 927 cm^{-1} become more obvious with increasing heat treatment time (Fig. 3c), indicating that the covalent bonding between the CDs and BA gradually enhanced. Meanwhile, the signal at 1189 cm^{-1} originated from an asymmetrically stretched oxygen atom connecting the trigonal boron atoms also become more remarkable [44]. In addition, as Figs. 3d-f and Table S4 (Supporting information) shown, with the extension of the reaction time, B−O band of UB-CD@BA powders gradually decrease while the contents of B_2O_3 and BCO_2 increase continuously in HR B 1s XPS spectra. We speculate that BA molecules occur self-polymerization with the prolongation of reaction time, which greatly increases the rigidity of the CD/BA system, resulting in strong fluorescent/phosphorescence emission. Noted that the intensities of fluorescence and phosphorescence emission dropped under longer time treatment (12 h), it might be because that further carbonization of UB-CD@BA at high time consumed the partial emissive species, and thereby affecting the optical properties of UB-CD@BA. In addition, we also investigated the effect of heat treatment temperature on the fluorescence/phosphorescence properties of UB-CD@BA (Fig. S9 in Supporting information). As the reaction temperature increased from 130 °C to 200 °C, the fluorescence and phosphorescence intensities of UB-CD@BA powders gradually increased, but exhibited sharp dropped under high reaction temperature of 400 °C. At low reaction temperature, only a small portion of BA chemically reacts with CDs, which leads to weak emission due to insufficient covalent bonding between BA and CDs. At high reaction temperature, excessive carbonization of UB-CD result in a decrease in the luminous intensity of UB-CD@BA.

Based on the above analysis, the formation process and high-efficiency solid-state luminescence origin of UB-CD@BA can be proposed as follows (Fig. 4). Under solvothermal conditions, the conjugated segments of perylene imide covalently fused to form large π-conjugation structure into CDs, which results in the long wavelength phosphorescent emission. During the thermal treatment the mixture of CDs and BA, covalent coupling reactions occurred between CDs and BA. Meanwhile, with the prolongation of the reaction time, the self-polymerization degree of the BA molecules deepened, forming a three-dimensional (3D) spatial restriction around CDs. The multi-confinement by strong 3D spatial restriction and stable covalent bonding can suppress the non-radiative transition and promotes intersystem crossing by restraining the vibrational freedom of the CDs. It also prevents aggregation-induced quenching in the solid state. These strong effects greatly promote the fluorescence and phosphorescence emission, especially for phosphorescence, thus leading to highly-efficiency and ultrabroadband pure white light emission.

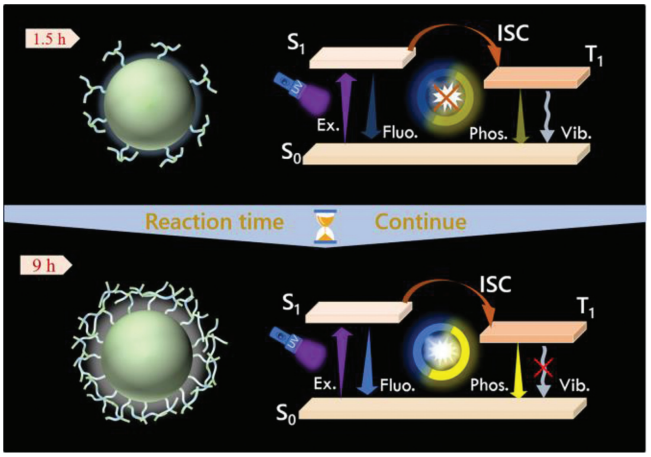

Fig. 4. Formation mechanism of efficient white light emission for UB-CD@BA powders (Ex.: Excite; Fluo.: Fluorescence; Phos.: Phosphorescence; Vib.: Vibration).

The ultra-wide spectral characteristic and high efficiency of UB-CD@BA strongly suggest that the UB-CD@BA holds potential in constituting super performance WLED. Since the photoluminescence emission spectrum of UB-CD@BA powders shows excellent CIE value under 395 nm excitation, UB-CD@BA were compatible with commercial 395 nm UV-LED chips to manufacture WLEDs.

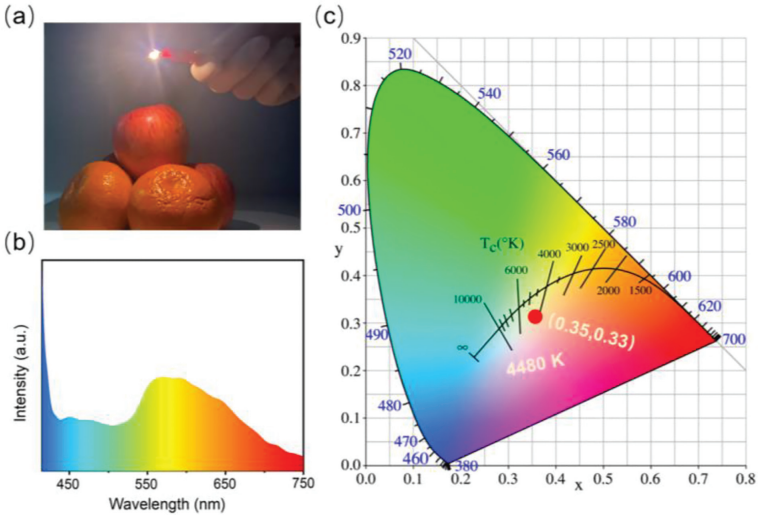

Fig. 5. (a) Photograph of the WLED lamp. (b) Electroluminescence spectrum of the WLEDs with InGaN UV (395 nm). (c) Calculated PL emission color coordinates in the CIE 1931 chromaticity diagram.

UB-CD@BA powders were wrapped in silicone glue and coated on UV-LED chip to form a WLED that can emit bright light enough to illuminate the fruits (Fig. 5a). Electroluminescence spectrum of the as-fabricated WLED shows two distinct peaks at 455 nm and 570 nm, which were attributed to blue fluorescence and yellow phosphorescence, respectively (Fig. 5b). In addition, as shown in Fig. 5c, the prepared WLED based on UB-CD@BA has favorable white light characteristics with a CCT value of 4480 K and CRI of 87. Moreover, the CIE coordinates is (0.35, 0.33), which is very close to the standard white light (0.33, 0.33).

In conclusion, we developed a convenient synthetic approach to obtain an efficient pure white light UB-CD@BA by thermal treatment of BA and CDs with large conjugated structure. The as-prepared UB-CD@BA exhibited strong fluorescence/phosphorescence dual emission, where the overall QY was as high as 28% and PQY reached up to 21%. Remarkable, the prepared UB-CD@BA powders showed the highest reported full width at half maximum of 250 nm. It has been revealed that the covalent coupling and confined effect played a significant role in producing the phosphorescence emission and preventing aggregation-induced quenching in the solid state. The single component WLED was prepared with UB-CD@BA powder as the color conversion layer, which showed favorable white light characteristics with a CCT value of 4480 K. In addition, its CIE coordinates and CRI reached (0.35, 0.33) and 87, respectively. This work offers a feasible synthetic approach for the preparation of strong pure white light emissive materials for single component WLEDs.

Declaration of competing interest

The authors declare that they have no known competing financial interests or personal relationships that could have appeared to influence the work reported in this paper.

Acknowledgments

The authors acknowledge the support from the National Natural Science Foundation of China (Nos. 52002152 and 62005106), the Natural Science Foundation of Jiangsu Province (Nos. BK20190864 and BK20190865), the Primary Research & Development Plan of Zhenjiang-Modern Agriculture (No. NY2021007). The authors would also like to sincerely thank Wang Ning from Shiyanjia Lab (www.shiyanjia.com) for the XPS analysis.

Supplementary materials

Supplementary material associated with this article can be found, in the online version, at doi:10.1016/j.cclet.2022.107794.

References

[1] S. Reineke, F. Lindner, G. Schwartz, et al., Nature 459 (2009) 234–238.
[2] X. Wang, X. Yan, W. Li, et al., Adv. Mater. 24 (2012) 2742–2747.
[3] S. Kim, T. Kim, M. Kang, et al., J. Am. Chem. Soc. 134 (2012) 3804–3809.
[4] X. Li, Y. Liu, X. Song, et al., Angew. Chem. Int. Ed. 54 (2015) 1759–1764.
[5] Y. Chen, M. Zheng, Y. Xiao, et al., Adv. Mater. 28 (2016) 312–318.
[6] H.S. Jang, H. Yang, S.W. Kim, et al., Adv. Mater. 20 (2008) 2696–2702.
[7] J. Li, Y. Tang, Z. Li, et al., ACS Nano 15 (2021) 550–562.
[8] D. Tu, P. Leong, S. Guo, et al., Angew. Chem. Int. Ed. 56 (2017) 11370–11374.
[9] Z. He, W. Zhao, J.W.Y. Lam, et al., Nat. Commun. 8 (2017) 416.
[10] X. Zhang, J. Yu, J. Wang, et al., ACS Appl. Mater. Inter. 7 (2015) 28122–28127.
[11] Q. Wang, M. Xie, X. Min, et al., Chem. Phys. Lett. 727 (2019) 72–77.
[12] B. Yan, C.C.C. Cheung, S.C.F. Kui, et al., Adv. Mater. 19 (2007) 3599–3603.
[13] M. Bowers, J. McBride, S. Rosenthal, J. Am. Chem. Soc. 127 (2005) 15378–15379.
[14] B. Yao, H. Huang, Y. Liu, et al., Trends Chem. 1 (2019) 235–246.
[15] J. Tan, Q. Li, S. Meng, et al., Adv. Mater. 33 (2021) e2006781.
[16] H. Li, Z. Kang, Y. Liu, et al., J. Mater. Chem. 22 (2012) 24230.
[17] C. Hu, M. Li, J. Qiu, et al., Chem. Soc. Rev. 48 (2019) 2315–2337.
[18] X. Bao, Y. Yuan, J. Chen, et al., Light-Sci. Appl. 7 (2018) 91.
[19] K. Jiang, L. Zhang, J. Lu, et al., Angew. Chem. Int. Ed. 55 (2016) 7231–7235.
[20] B. Zhao, Z. Tan, Adv. Sci. 8 (2021) 2001977.
[21] Q. Li, M. Zhou, M. Yang, et al., Nat. Commun. 9 (2018) 734.
[22] B. Wang, Z. Sun, J. Yu, et al., SmartMat 3 (2022) 337–348.
[23] G. Gao, Y. Jiang, W. Sun, et al., Chin. Chem. Lett. 29 (2018) 1475–1485.
[24] B. Wang, S. Lu, Matter 5 (2022) 110–149.
[25] J. Zhu, J. Hu, Q. Hu, et al., Small 18 (2022) e2105415.
[26] H. Zhang, K. Liu, J. Liu, et al., CCS Chem. 2 (2020) 118–127.
[27] J. Tan, R. Zou, J. Zhang, et al., Nanoscale 8 (2016) 4742–4747.
[28] K. Jiang, X. Gao, X. Feng, et al., Angew. Chem. Int. Ed. 59 (2020) 1263–1269.
[29] Q. Li, M. Zhou, Q. Yang, et al., Chem. Mater. 28 (2016) 8221–8227.
[30] J. Tan, Y. Ye, X. Ren, et al., J. Mater. Chem. C 6 (2018) 7890–7895.
[31] W. Liu, K. Ng, H. Lin, et al., J. Lumin. 242 (2022) 118606.
[32] T. Yuan, F. Yuan, X. Li, et al., Chem. Sci. 10 (2019) 9801–9806.
[33] Z. Wang, Y. Liu, S. Zhen, et al., Adv. Sci. 7 (2020) 1902688.
[34] Q. Li, Y. Li, S. Meng, et al., J. Mater. Chem. C 9 (2021) 6796–6801.
[35] P. Karuppuswamy, H. Chen, P. Wang, et al., ChemSusChem 11 (2018) 415–423.
[36] G. Dong, L. Yang, F. Wang, et al., ACS Catal. 6 (2016) 6511–6519.
[37] L. Yang, G. Dong, D. Jacobs, et al., J. Catal. 352 (2017) 274–281.
[38] Z. Zhang, X. Chen, H. Zhang, et al., Adv. Mater. 32 (2020) e1907746.
[39] X. Yang, L. Sui, B. Wang, et al., Sci. China Chem. 64 (2021) 1547–1553.
[40] X. Chen, X. Zhang, F. Wu, Chin. Chem. Lett. 32 (2021) 3048–3052.
[41] B. Wang, Z. Wei, L. Sui, et al., Light-Sci. Appl. 11 (2022) 172.
[42] W. Deng, H. Yang, Y. Shen, et al., ACS Appl. Mater. Inter. 7 (2015) 21095–21099.
[43] Q. Li, Z. Zhao, S. Meng, et al., SmartMat 3 (2022) 260–268.
[44] W. He, X. Sun, X. Cao, ACS Sustain. Chem. Eng. 9 (2021) 4477–4486.
[45] W. Li, W. Zhou, Z. Zhou, et al., Angew. Chem. Int. Ed. 58 (2019) 7278–7283.
[46] L. Wang, W. Li, L. Yin, et al., Sci. Adv. 6 (2020) eabb6772.
[47] Z. Sheng, H. Gao, W. Bao, et al., J. Mater. Chem. 22 (2012) 390–395.